



Two Novel Predictive Networks for Slope Stability Analysis Using a Combination of Genetic Programming and Artificial Neural Network Techniques

Hossein Moayed^{1,2} 

¹ Institute of Research and Development, Duy Tan University, Da Nang 550000, Vietnam
hosseinmoayed@duytan.edu.vn

² Faculty of Civil Engineering, Duy Tan University, Da Nang 550000, Vietnam

Abstract. The stability of slopes is an important parameter which can affect many engineering projects. In this study, we employed genetic programming (GP) and artificial neural network (ANN) techniques, based on upper bound (UB) limit analysis, for the problem in designing solution charts for slope stability. Existing theories of genetic programming predictive network models have not been applied in the area of slope stability. Accordingly, the main objective of this research is to propose a new GP model to estimate the factor of safety parameter and providing design solution charts in a two-layered cohesive slope. A dataset containing 400 UB analysis models was used to train and test the GP and ANN networks. Variables of the GP algorithm training network parameters and weights such as population size, number of genes, and tournament size were optimized. The input includes d/H , (depth factor), the undrained shear strength ratio (C_{u1}/C_{u2}), and slope angle (β), where the output was taken as a dimensionless stability number (N_{2c}). The predicted results for both datasets (training and testing) from the GP and ANN models were evaluated based on two statistical indexes (root mean square error, RMSE, and coefficient of determination, R^2). Besides, the obtained results were compared with actual values of N_{2c} , in the form of design charts. The results show that both the GP and ANN models are accurate enough to be used in this field. Also, ANN performed slightly better than the GP. As a result, a formula was derived for each GP and ANN models to assess the slope stability behaviors of two-layered cohesive soils.

Keywords: Artificial neural network · Genetic programming · Optimization algorithm · Slope stability

1 Introduction

The slope stability problem has been studied for years, being of considerable concern due to its effects on geotechnical designs [1]. Generally, slopes are categorized as a cut slope, natural slope or fill slope, and physical and geometric factors influence their

stability. Also, the parameters which are related to soil strength affect the slope behavior too. The safety factor (F_s) of a cohesive slope is related to a well-recognized parameter named the dimensionless stability number (N_{2c}). One of the first studies that led to the development of useful design charts for the slope stability issue was implemented by Taylor [2]. More recently, various research studies have concentrated on providing design chart solutions (e.g., Qian et al. [3], Abuel-Naga et al. [4], Aksoy et al. [5] and Moayedi and Hayati [6]). Some time and cost constraints are constraints of using the new advances in mathematical and computer modeling tools. Therefore, the importance of providing the design charts is becoming more highlighted. As a novel idea, intelligent predictive tools (i.e., artificial neural networks (ANNs) and particle swarm optimization (PSO)) are being employed for the subject of slope stability evaluation [7, 8]. Jiang et al. [9] applied the UB method to investigate a rock slope's seismic behavior and safety factor with a tunnel. As a result, they found three factors, namely the horizontal seismic force coefficient, the slope height, and the internal friction angle, to be the most influential parameters influencing the safety factor's sensitivity. In another study, Pan and Dias [10] assessed the face stability for the case of a non-circular tunnel through an upper bound limit analysis model, synthesized with the technique of strength reduction. According to their results, this approach presents conservative results and can be applied in safety factor evaluation in a particular design.

The number of studies concerned about the feasibility of neural network modeling to solve slope stability is limited. The hybrid GP model that is presented in this study has not been proposed for the problem of slope stability previously. There is almost no study on using hybrid GP-based learning systems to predict the factor of safety and its key parameters. In the following, the GP prediction models' results were compared with the results of an optimized ANN feedforward learning system. Similarly, to find the best ANN structure, all the proposed models were evaluated with a trial and error process on their influential parameters. Finally, each model's design chart solution was depicted; and the formula was presented for both the GP and ANN models to be used for slopes with the same conditions. In this paper, optimal forms of genetic programming (GP) and ANN models have been utilized to predict the N_{2c} in a two-layered cohesive slope, based on the upper bound (UB) limit analysis method. The UB model is broadly applied for similar engineering problems. The slope proposed for this work was constructed from two separate clayey layers, lying on a rigid rock bed. The ratio of the first soil layer thickness to the full height of the slope, d/H , the slope angle, β , and the ratio of the undrained shear strength of the first soil layer to that of the slope layer, C_{u1}/C_{u2} , were considered as three efficacious parameters that affect the slope situation. These parameters also form the input dataset. Meanwhile, the N_{2c} was taken as the output of the networks. 80% of the dataset was devoted to the training part, and the remaining 20% was selected to test the networks.

2 Artificial Intelligence Systems

Genetic Programming. Genetic programming is a powerful computing technology that has been initiated based on genetic algorithms (GA). This model was first introduced in 1985 by Cramer [11]. Another scholar, Ref Koza, later improves it in 1984 [12]. It

is widely used in solving engineering problems by numerous scholars such as Johari et al. [13], Makkeasorn et al. [14], Garg et al. [15], and Garg et al. [16]. During the GP process, particular computer programs are applied to predict the problem’s potential outputs by linking the input data layers and main output(s). One of the critical issues in using the GP algorithm is that the user will have a simpler finalized algorithm. The overall procedure of GP prediction performance is illustrated in Fig. 1. The complete detail of the applied GP technique is well described in Ref. [12, 15–17].

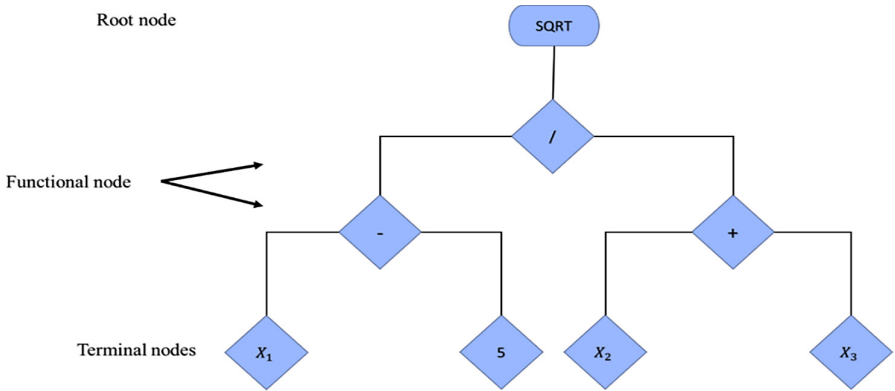


Fig. 1. Typical GP tree presented for the function $[(X1-5)/(X2 + X3)]^2$

Artificial Neural Network. The artificial neural networks (ANNs), which mainly inspired by a biological neural network, are well established as one of the most applicable approaches that have been employed in the last two decades is, which were first introduced by McCulloch and Pitts [18]. These tools are widely employed for prediction purposes [19]. Numerous scholars such as Rao [20], El-Bakry [21], Samui and Kumar [7], and Moayedi and Hayati [22] are experiences successful use of ANN in predicting complex engineering solutions. Overall, the primary objective is to establish a non-linear equation (i.e., trained based on the initial learning process) between the inputs and output(s) dataset [20]. In this sense, a neural network’s typical architecture is prepared according to components of so-called neurons. As illustrated in Fig. 2, the input layer includes layers of the input(s) data. As a predefined model, the number of nodes is considered the same as the input parameters. During the neural network training processes, there can be one or more hidden layer(s) finally, and the calculation process will end to one or more output layer(s). More precisely, for each node, if we assume the term X as the main input and the term W as the interconnected weight (which is also shown as I_w), the bias (which is shown by the term of β) will be added to the summation of WXs . In this regard, an activation function ($f(I)$) will be applied to the acquired term $(\sum \mathbf{WX} + \beta)$ to produce the outputs. The activation function for this case was considered as Tan-sigmoid (Tansig) which is defined by Eq. (1):

$$Tansig(x) = \frac{2}{1 + e^{-2x}} - 1 \tag{1}$$

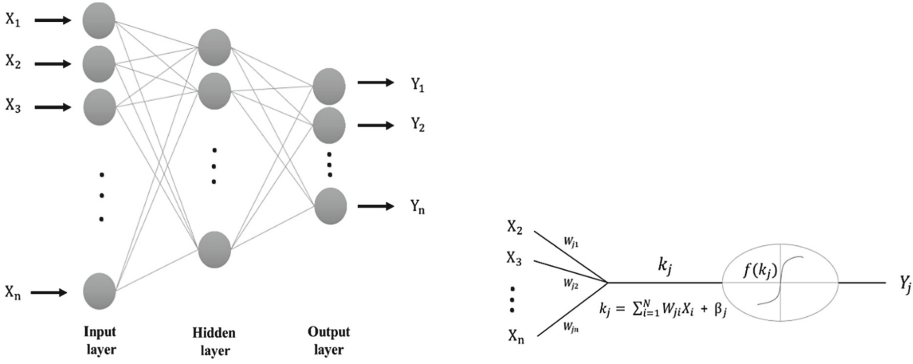


Fig. 2. Typical structure and operation of ANNs

3 Data Collection and Problem Statement

In this research, the results from the upper bound (UB) type of limit analysis method were employed to assess the short-term stability situation of a cohesive slope. This method is well discussed in other studies (e.g., Florkiewicz [23], Donald and Chen [24], Karkanaki et al. [25], and Jiang et al. [9]). The slope is constructed from a maximum of two different soil layers with separate material properties lying on a bedrock layer in the present case. Besides, Fig. 3 shows a graphical description of the input data range versus the data numbers for d/H , the slope angle of β° and the C_{u1}/C_{u2} ratio. The analysis is performed with new computer software called *OptumG2*. It is based on finite element limit analysis and has been widely used in other studies (e.g., Karkanaki et al. [25]; Caër et al. [26] and Zhou et al. [27]). The analytical method used and the 2D boundary conditions applied in this study, i.e., to illustrate the pure cohesive slope, are similar to the research performed by Qian et al. [3]. A view of the slope model is presented in Fig. 4. As can be obtained from this figure, the proposed slope has been formed from two cohesive soil layers having only consistent undrained strength (c_{ul}) with a zero undrained internal friction angle. C_{u1} and C_{u2} , respectively define the undrained cohesive strength for the top and bottom soil layers. The influential parameters and an example of output from *OptumG2* are illustrated in Figs. 4a and 4b, respectively.

4 Model Development for Prediction of N_{2c}

A proper estimation process, which is used by hybrid ANN models, should be formed from several steps such as (i) data processing and normalization, (ii) selecting a suitable hybrid model, and finally (iii) finding an appropriate hybrid structure for the proposed model, which can be achieved through a trial and error procedure. For the aim of producing the design chart solutions, N_{2c} (a dimensionless stability number, which was first investigated by Taylor [2]) was obtained from Eq. (2):

$$N_{2c} = c_{u1} / \gamma HF_s \tag{2}$$

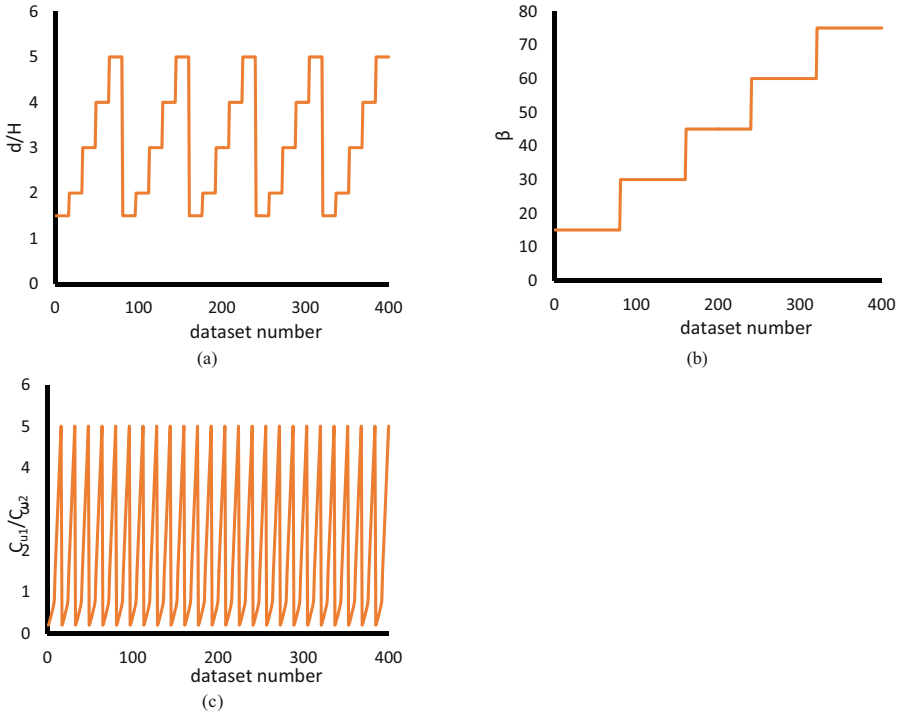


Fig. 3. Graphical description of the range of input data versus data numbers for (a) d/H , (b) slope angle, (c) C_{u1}/C_{u2}

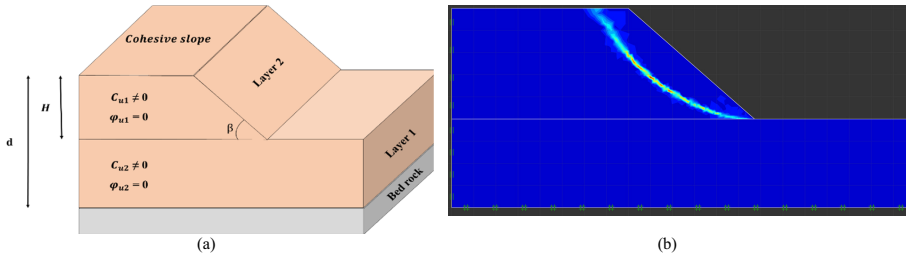


Fig. 4. A view of the model for cohesive slope (a) schematic model, (b) OptumG2 stability output for upper bound limit analysis

where N_{2c} , C_{u1} , and F_s define the dimensionless stability number, the undrained shear strength of the second soil layer, and the factor of safety obtained from the OptumG2 modeling, respectively. Also, γ describes the soil unit weight, which is taken as 20 kN/m^3 .

The dataset used is constructed from three inputs: the three influential parameters affecting the slope stability situation. The first factor is related to depth (d/H). It defines the ratio of both soil layer thicknesses, d , to the slope’s top layer height, H . The angle

of the present slope (β) was considered the second parameter. The third effective factor defines the undrained shear strength ratio (C_{u1}/C_{u2}). An example of the mentioned data is presented in Table 1. Note that these values are derived from the OptumG2 simulation, and, as illustrated, the three useful parameters of d/H , β , and C_{u1}/C_{u2} are employed to estimate the N_{2c} in the three FEM methods of LB, UB, and LEM limit analysis.

Table 1. Example of inputs and output dataset applied for modeling purpose

Model number	Inputs			Output N_{2c} -UB limit analysis	Model number	Inputs			Output N_{2c} -UB limit analysis
	d/H	β°	C_{u1}/C_{u2}			d/H	β°	C_{u1}/C_{u2}	
1	5	75	5	0.7779	26	3	75	4.5	0.6295
2	5	60	5	0.7663	27	5	45	4	0.6276
3	5	45	5	0.7605	28	5	30	4	0.6227
4	5	30	5	0.7547	29	4	15	4.5	0.6179
5	4	75	5	0.7450	30	4	75	4	0.6140
6	4	60	5	0.7275	31	3	60	4.5	0.6101
7	5	15	5	0.7246	32	4	60	4	0.6053
8	4	45	5	0.7217	33	3	45	4.5	0.6024
9	4	30	5	0.7139	34	5	15	4	0.6004
10	5	75	4.5	0.7091	35	4	45	4	0.5995
11	5	60	4.5	0.6994	36	2	75	5	0.5966
12	5	45	4.5	0.6945	37	4	30	4	0.5936
13	3	75	5	0.6936	38	3	30	4.5	0.5898
14	5	30	4.5	0.6887	39	3	15	5	0.5839
15	4	75	4.5	0.6780	40	5	75	3.5	0.5733
16	4	15	5	0.6722	41	3	75	4	0.5684
17	4	60	4.5	0.6664	42	5	60	3.5	0.5645
18	5	15	4.5	0.6635	43	4	15	4	0.5626
19	4	45	4.5	0.6615	44	5	45	3.5	0.5597
20	3	60	5	0.6615	45	3	60	4	0.5578
21	4	30	4.5	0.6548	46	5	30	3.5	0.5548
22	3	45	5	0.6518	47	3	45	4	0.5510
23	5	75	4	0.6412	48	4	75	3.5	0.5510
24	3	30	5	0.6383	49	2	60	5	0.5451
25	5	60	4	0.6324	50	2	75	4.5	0.5432

5 Results and Discussion

The present study intends to evaluate the stability of a two-layered cohesive slope by using two intelligent techniques. An MLP neural network and a GP mode were applied to approximate the stability of the slope. The important parameter of the dimensionless stability number (N_{2c}) was considered the networks' output. It was estimated to be influenced by three effective factors, which were considered as (i) the layer's height ratio (d/H), (ii) the slope angle (β), and (iii) the undrained cohesive strength ratio (C_{u1}/C_{u2}) as the input dataset. Similar to previous research, the stock dataset was randomly divided into two parts to train and test the networks, with a ratio of 80% and 20%, respectively (e.g., Moayedi and Hayati [28], Moayedi and Hayati [22], Koopialipour et al. [29] and Moayedi and Hayati [6]). Also, for each model, the performance was measured by the index of the statistical error terms RMSE and R^2 . Equations (3) and (4) explain these indices:

$$RMSE = \sqrt{\frac{1}{N} \sum_{i=1}^N [(Y_{i_{actual}} - Y_{i_{produced}})]^2} \quad (3)$$

$$R^2 = 1 - \frac{\sum_{j=1}^N [(Y)_{actual,j} - (Y)_{produced,j}]^2}{\sum_{j=1}^N [(Y)_{actual,j} - (Y)_{mean}]^2} \quad (4)$$

Where $Y_{i_{actual}}$ and $Y_{i_{produced}}$ stand for the actual and predicted values of N_{2c} , respectively. N is the indicator of the number of data, and Y_{mean} is the average of the actual slope stability values. The mentioned indices have been widely used in other earlier studies (e.g., Momeni et al. [30], Armaghani et al. [31], Mohamad et al. [32] and [33]).

Optimal Hybrid GP Model Predicting N_{2c} . Determining proper network architecture is a necessary step in the utilization of artificial intelligence. For GP optimization, many trial and error processes, including 36 various GP models, were performed to find an appropriate GP structure for estimating the N_{2c} . The feasibility of the GP technique was evaluated for different numbers of generations, values of swarm sizes, and selection tournament sizes. For all three mentioned parameters, 12 values, including 50, 100, 150, 200, 250, 300, 350, 400, 450, 500, 750, and 1000 were considered, and the performance was evaluated by means of the RMSE reduction procedure. Regarding the trial and error processes provided in Figs. 5, 6 and 7, the GP model with the values of 750, 200, and 250 respectively for the population size, some generations and selection tournament size showed the best performance, as indicated by its lower RMSE value. Therefore, this structure was introduced as the optimal architecture of the GP for any further N_{2c} estimation.

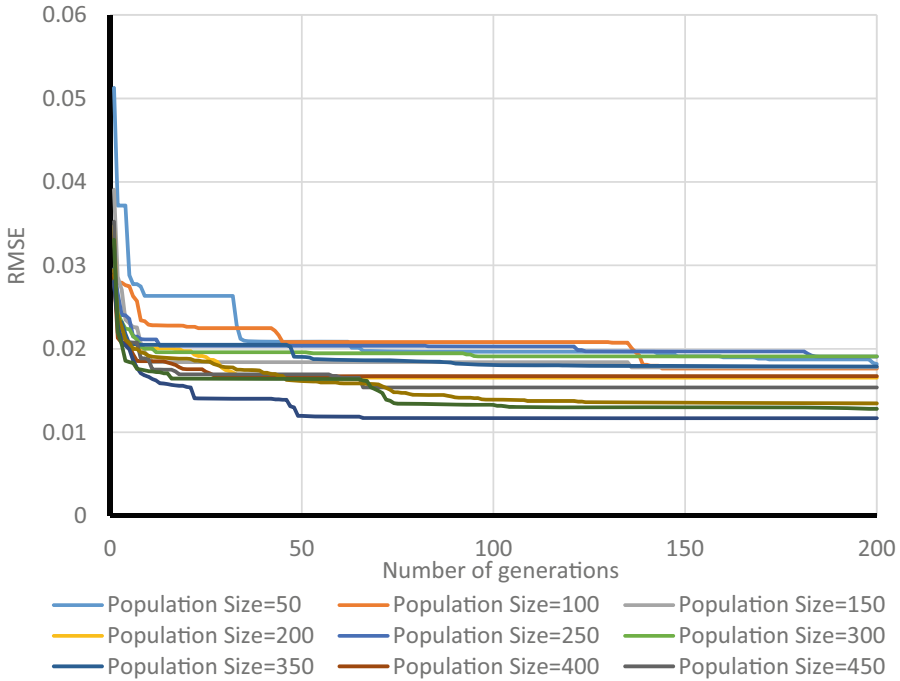


Fig. 5. GP network performance results for different population sizes

Optimal Artificial Neural Network Predicting N_{2c} . Like the GP model, the best ANN architecture was obtained by assessing several ANN structures' performance. For the ANN, a multilayer perceptron network was verified with various numbers of neurons in its single hidden layer. After a trial and error process, the network that reported the lowest RMSE and the highest R^2 was selected as the optimum model. The results of this are depicted in Fig. 8. Note that every structure was performed for six iterations. As a general deduction, the MLP network with at least eight neurons in its hidden layer could present an accruable performance for modeling the problem.

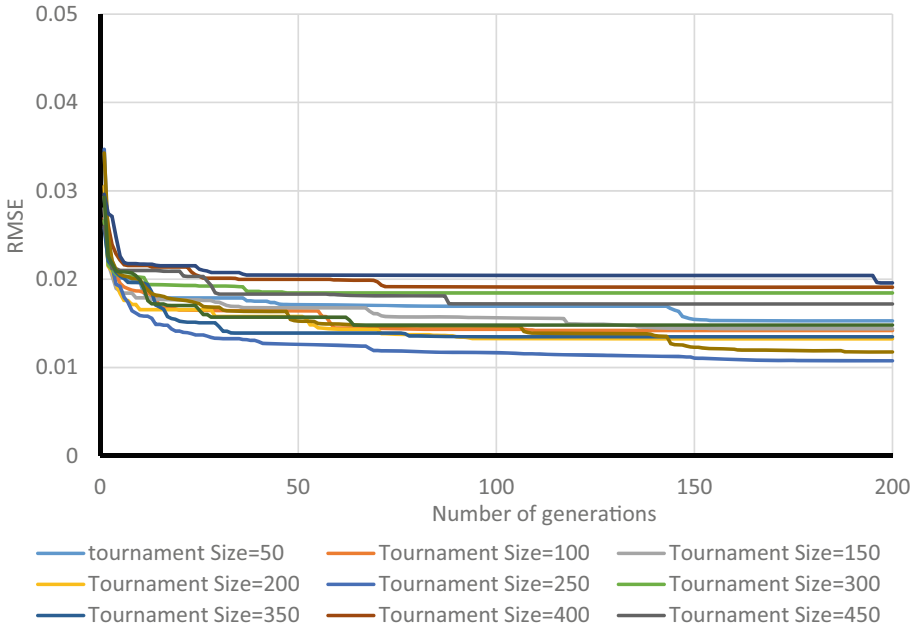


Fig. 6. GP network performance results for different tournament sizes

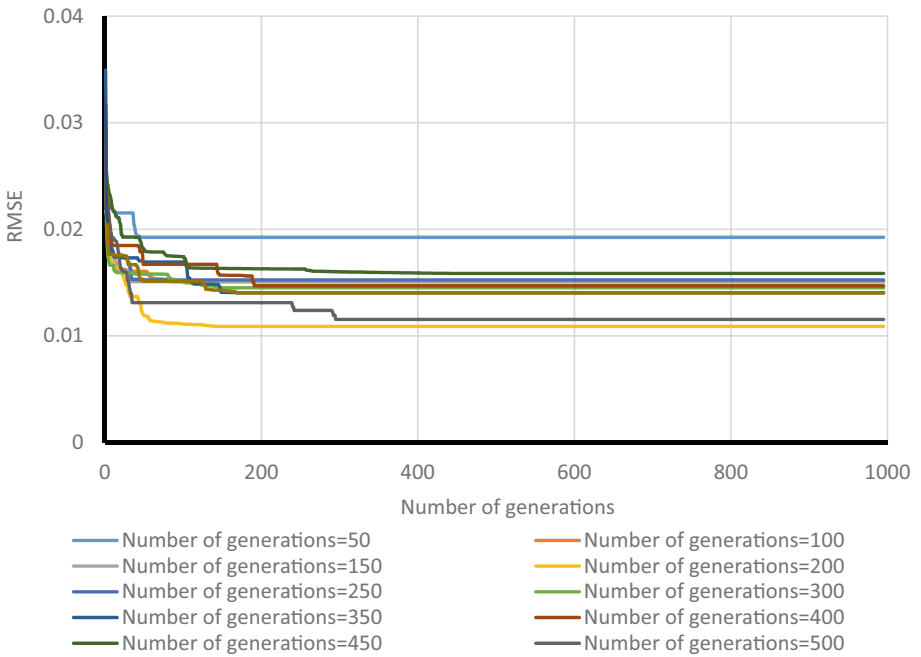


Fig. 7. GP network performance results for a different number of generations

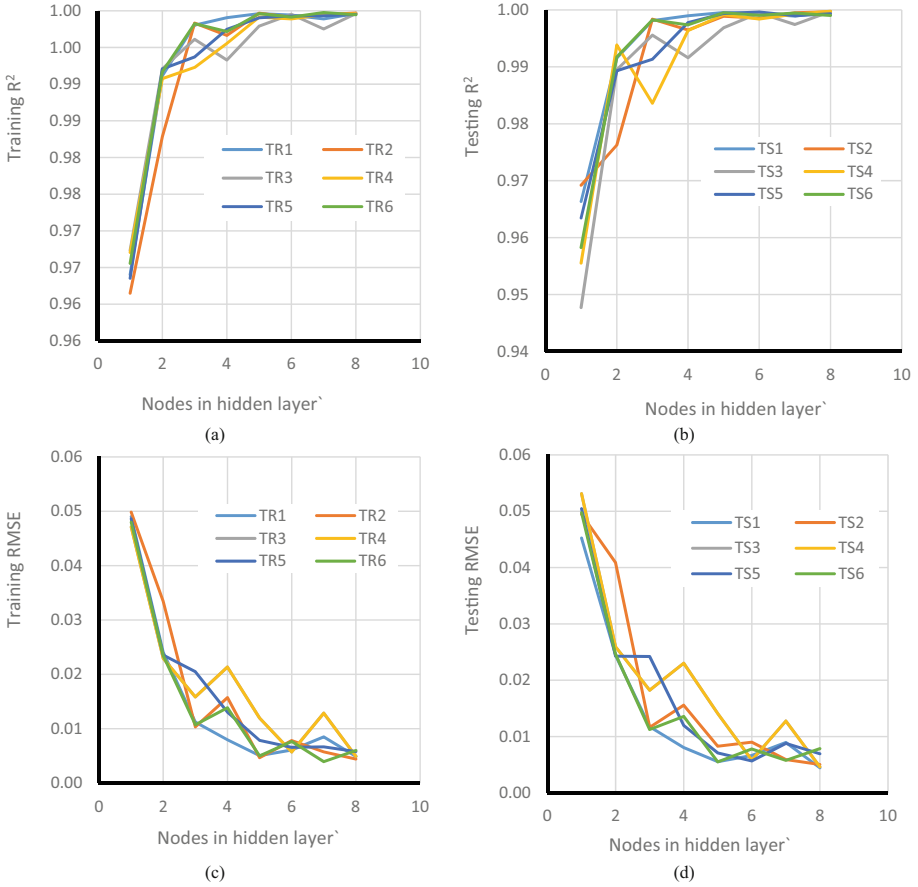


Fig. 8. Sensitivity analysis for ANN, based on (a) R^2 and (b) RMSE values reported for training and testing datasets

6 Models Evaluation and Design Solution Charts

After obtaining the optimum structures of both the GP and ANN methods, they were applied to the prepared dataset for the proposed estimation of the dimensionless slope stability number. The training dataset did a training operation, and the performance of each model was evaluated using the testing data. Two usual types of charts were used to describe and analyze the results. Firstly, the accommodation of the predicted and actual values of N_{2c} was depicted in the form of Fig. 9. Also, Table 2 lists the calculated RMSE and R^2 . As illustrated in Fig. 9 and Table 2, the GP and ANN models had a robust prediction and sufficient reliability in the slope stability assessment. The high values of R^2 can prove this claim, and the low values of RMSE obtained from both model performances. The training results show RMSE of 0.010274 and 0.006112 and R^2 of 0.9968 and 0.9989 for the GP and ANN methods. The results of the test phase show a good approximation for these models too. The RMSE and R^2 values are 0.011146 and 0.005927, and 0.9967 and 0.9990, respectively, for the GP and ANN methods. Based on the reported results, the optimized ANN had a slightly better performance compared to the optimized GP model, as can be concluded from the lower RMSE and higher R^2 values in both the training and testing phases.

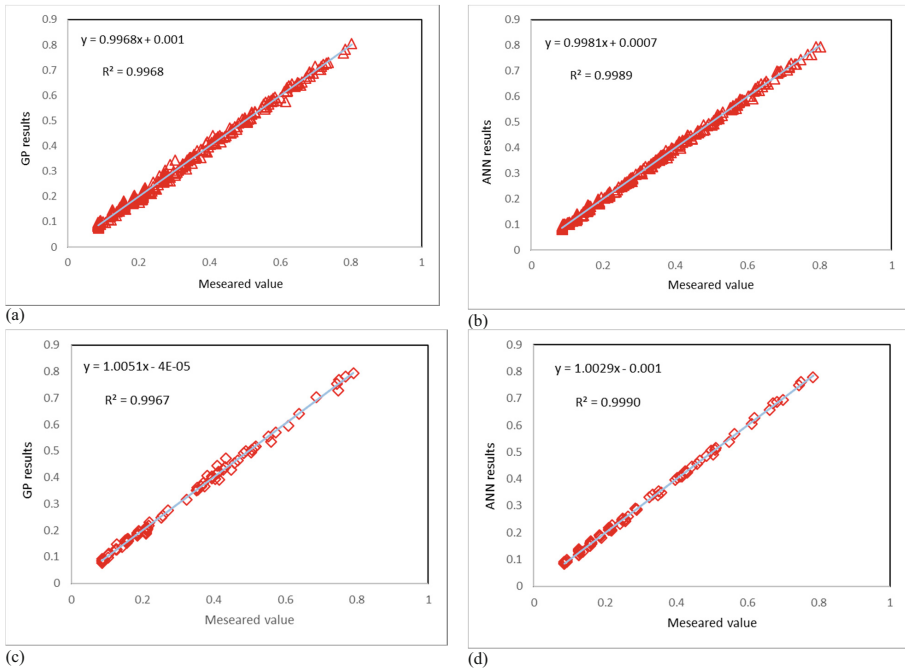


Fig. 9. Training (a and b) and testing (c and d) results of GP and ANN models for predicting N_{2c}

In the following, the measured results from the upper bound analysis of slope stability are compared with the predicted values obtained from the optimal GP and ANN

Table 2. Obtained RMSE and R^2 values for GP and ANN results

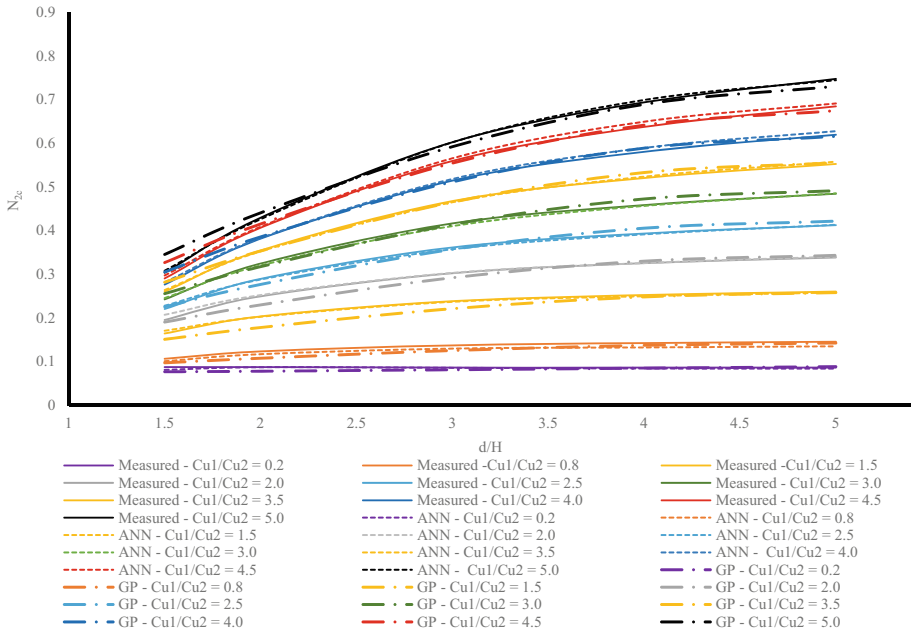
Model	Dataset			
	RMSE	R^2	RMSE	R^2
GP	0.010274	0.9968	0.011146	0.9967
ANN	0.006112	0.9989	0.005927	0.9990

algorithms. Consequently, Figs. 10-a to 10-e present the measured N_{2c} as well as the results obtained from the GP and ANN training networks for slope angles between 15 to 75°, respectively. In this regard, according to the different values of the slope angle (β) (i.e., 15°, 30°, 45°, 60° and 75°), separate solution of designing slope stability charts were provided, noting that in each figure the vertical and horizontal axes stand for the N_{2c} and d/H ratio, respectively. To include the C_{u1}/C_{u2} ratio parameter, C_{u1}/C_{u2} ratios of 0.2, 0.8, 1.5, 2, 2.5, 3, 3.5, 4, 4.5, and 5 were considered through the calculation steps. Therefore, ten different curves are plotted for each of the predefined slopes.

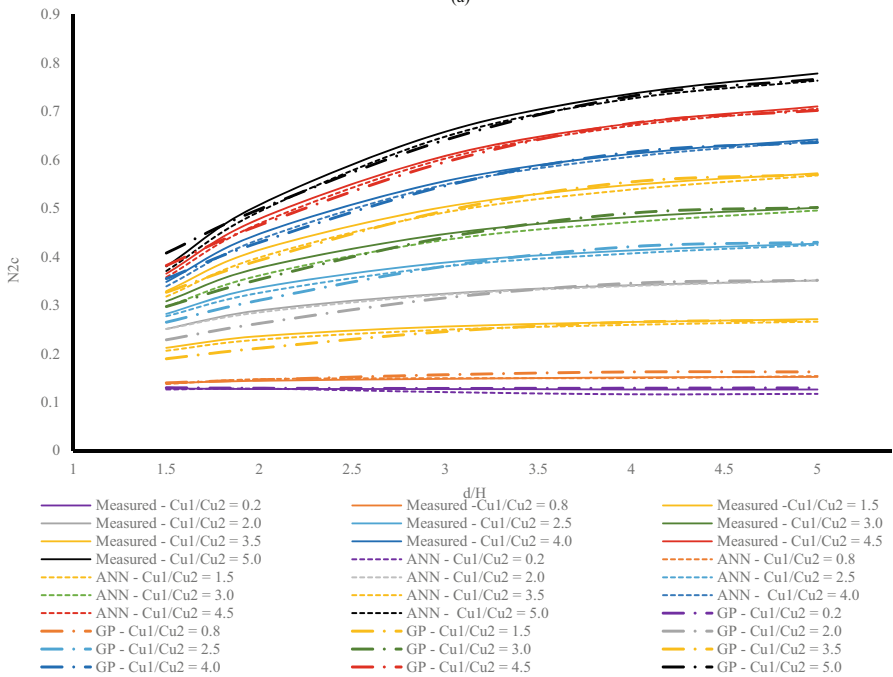
The curves showing $C_{u1}/C_{u2} = 0.2$ to 0.8 are drawn in a relatively straight path, and the N_{2c} does not show noticeable changes as the d/H ratio rises. In contrast, for the remaining eight curves (especially for $C_{u1}/C_{u2} = 3$ to $C_{u1}/C_{u2} = 5$), the N_{2c} values have an ascending direction as the d/H ratio rises. Note that the distance between these two curves decreases as β rises so that in the last graph ($\beta = 75^\circ$), they have covered each other. Also, there is another difference in the last graph. It relates to the fluctuations of the curves (especially for the curves determined by $C_{u1}/C_{u2} = 3.5, 4,$ and 5). In graphs, a – d, a steeper tangent can be observed for d/H values less than 2.5, while it differs for graph e, and camber can be seen in the vicinity of $d/H = 2$ (especially for $C_{u1}/C_{u2} = 5$).

As can be obtained from Figs. 10a–e, both the GP and ANN models gave a satisfactory prediction for estimating the slope stability number. This can be concluded from the GP and ANN curves' appropriate proximity to the measured N_{2c} (target data). It is worth noting that each target curve's general direction is well approximated by both the GP and ANN tools. Therefore, there is good coverage for all of them.

Focusing on the measured datasets, considering the black and red curves in Figs. 10a–e ($C_{u1}/C_{u2} = 4.5$ and 5), there are fluctuations and sudden changes for the N_{2c} results provided for d/H ratios, which are lower than 2.0. To evaluate the GP and ANN's flexibility, it is necessary to compare their reactions against these changes. In cases a–d, it is observed that the GP model had maintained its main direction without significant changes, even for critical d/H ratios (see red and black dash-dot curves). On the contrary, the changes are well distinguished by the ANN curves, especially for the black curves in Figs. 10a–d. In each case, the fluctuation is well followed by the ANN, and there is excellent accommodation between them. Also, for the changes occurring in Fig. 10e ($\beta = 75^\circ$), the ANN gave a better approximation, and this is because its curve is closer to the target curve. For another example, the ANN's higher precision can be deduced considering the grey curve ($C_{u1}/C_{u2} = 2$) in cases a–c, while more distance between the measured and predicted curves are reported for the GP. Regarding these descriptions and also the obtained RMSE and R^2 values, it can be concluded that both the GP and



(a)



(b)

Fig. 10. Chart solutions for GP and ANN models for (a) $\beta = 15^\circ$, (b) $\beta = 30^\circ$, (c) $\beta = 45^\circ$, (d) $\beta = 60^\circ$, (e) $\beta = 75^\circ$

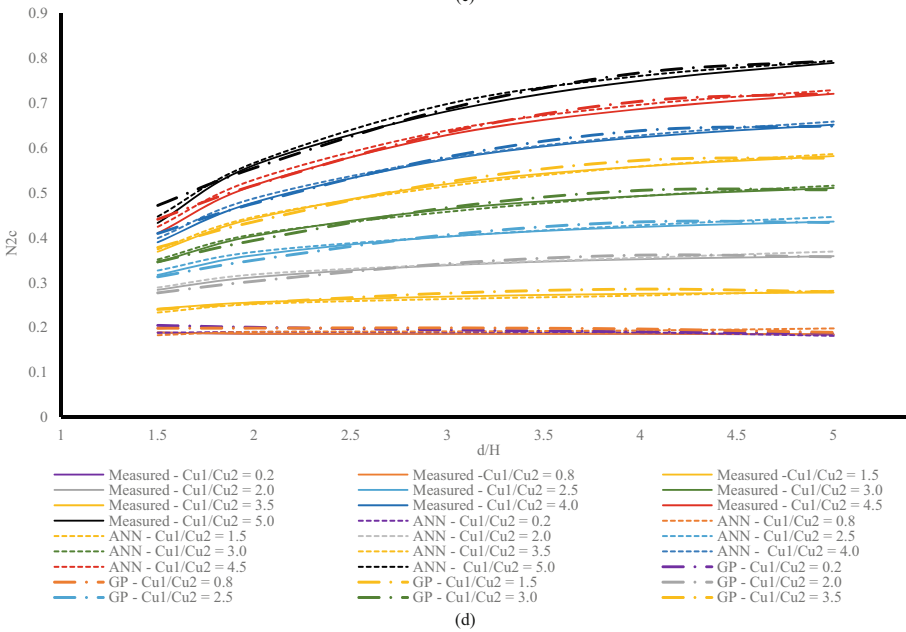
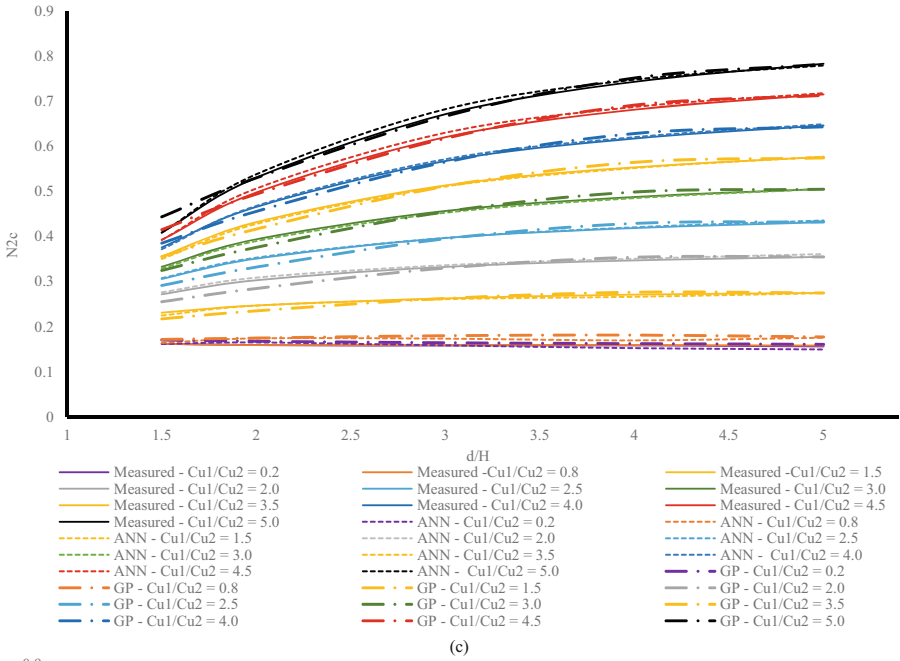


Fig. 10. (continued)

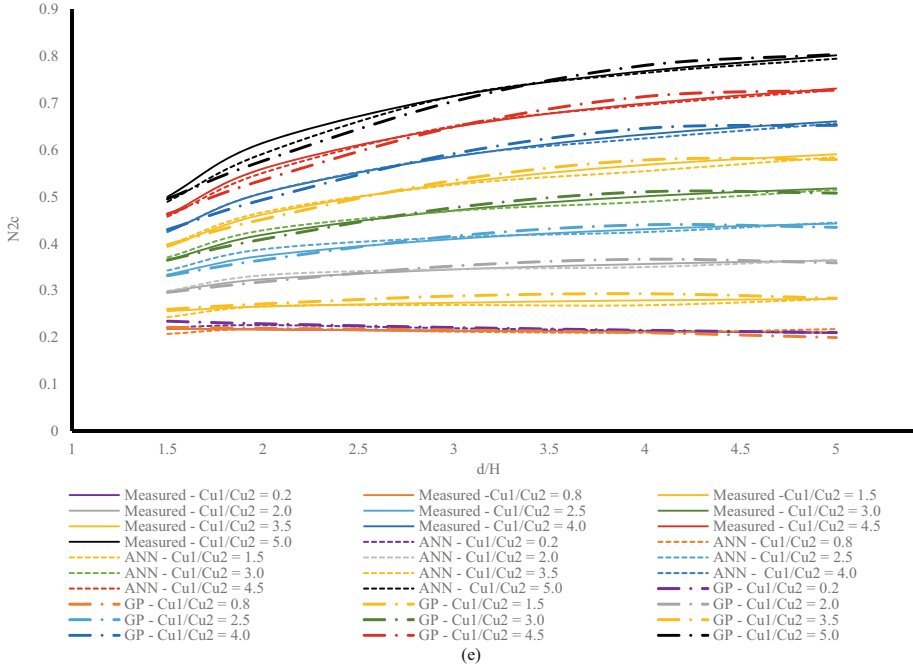


Fig. 10. (continued)

ANN models have sufficient applicability. Besides, the higher flexibility of the ANN in design solution charts can be concluded due to its response against the changes.

To provide a reliable solution equation that reflects the presented design charts, an equation was derived from both the GP and ANN trained networks to be presented in respect of the slope stability issue. The GP and ANN formulas are presented in Eqs. (5) and (6), respectively.

$$N_{2c-GP} = \frac{1510945278173245 \times (X_2 - (2 \times X_3))^{0.5}}{36028797018963968} + \frac{3659972446534761 \times X_1 \times \exp(X_3^{0.5})}{576460752303423488} - \frac{1628893347471811 \times X_1 \times X_3^{0.5} \times (X_3 - 86877) \times (89986 \times X_3 - X_1 \times X_3)}{2305843009213693952} - \frac{1145219825319659 \times X_1^{0.5} \times X_3^{0.5} \times (\sin(X_3) - X_2^{0.5}) \times (X_3 - 85851)}{576460752303423488} - 0.071172 \quad (5)$$

Where, $X_1 = d/H$; $X_2 = \beta$; and $X_3 = Cu1/Cu2$.

$$N_{2c-ANN} = -0.0726 \times Y_1 + 2.6658 \times Y_2 - 3.5444 \times Y_3 + 0.0117 \times Y_4 - 0.2708 \times Y_5 \times 1.1120 \times Y_6 - 0.0299 \times Y_7 - 0.1273 \times Y_8 - 0.7090 \quad (6)$$

Where, $Y_1, Y_2 \dots Y_8$ are defined by Eqs. 7–14:

$$Y_1 = \text{Tansig}(-1.0821 \times X_1 - 0.4887 \times X_2 + 2.6243 \times X_3 + 3.1157) \quad (7)$$

$$Y_2 = \text{Tansig}(0.1386 \times X_1 - 0.1071 \times X_2 + 0.6546 \times X_3 - 0.4376) \quad (8)$$

$$Y3 = \text{Tansig} (0.0804 \times X1 - 0.0947 \times X2 + 0.2168 \times X3 - 0.0942) \quad (9)$$

$$Y4 = \text{Tansig} (2.3293 \times X1 - 2.0853 \times X2 + 2.2883 \times X3 - 0.0371) \quad (10)$$

$$Y5 = \text{Tansig} (-0.0285 \times X1 + 0.3638 \times X2 - 3.0985 \times X3 - 1.5416) \quad (11)$$

$$Y6 = \text{Tansig} (0.9039 \times X1 + 0.3419 \times X2 - 0.7021 \times X3 + 1.9361) \quad (12)$$

$$Y7 = \text{Tansig} (-1.6865 \times X1 + 3.3371 \times X2 + 0.3808 \times X3 - 1.6126) \quad (13)$$

$$Y8 = \text{Tansig} (-3.1807 \times X1 + 0.8723 \times X2 + 0.8388 \times X3 - 4.1277) \quad (14)$$

where in each equation, $X1 = d/H$; $X2 = \beta$; $X3 = Cu1/Cu2$.

It is important to note that the proposed formula can be used in the slope stability problem to calculate the dimensionless stability number for slopes with a maximum of two layers with similar material conditions. Besides, there are two crucial advantages for the GP model equation compared with that of the ANN. One of them is the GP equation, which is easier to use than the ANN equation (i.e., the intermediate equations of Y1 to Y8 need to be considered before Eq. (6) can be used). The other is the GP equation that can be used directly and requires no normalization process (while in the ANN, the input layers need to be normalized before any further process).

7 Conclusions

Regarding the importance of the slope stability issue in many engineering projects, the main objective of this research was to evaluate the capability of two artificial intelligence techniques in the assessment of cohesive slope stability. Optimized GP and optimized ANN methods were applied to the dataset collected from a finite-element procedure called upper bound (UB) limit analysis. Three effective factors to the cohesive slope's stability were considered as input data to produce the dimensionless stability number. The first factor was the d/H ratio, where d is the slope thickness, and H is an indicator of the topsoil layer's height. Slope angle (β) was the second factor, and the third parameter was the ratio of the undrained shear strength of the first soil layer to the slope layer's ($Cu1/Cu2$). Besides the use of the statistical indices of RMSE and R^2 , the results were compared by the form of design charts solution. From the results, both the RMSE and R^2 values showed a slightly better approximation for the ANN than for the GP model in training (RMSE of 0.010274 and 0.006112, and R^2 of 0.9968 and 0.9989, respectively for the GP and ANN methods) and testing (RMSE of 0.011146 and 0.005927, and R^2 of 0.9967 and 0.9990, respectively for the GP and ANN methods) phases. We also found the ANN to be the more reliable model based on the reported results from the design charts.

Regarding these charts, the ANN showed higher flexibility in fluctuations. In the following, two formulas were extracted based on each of the optimized GP and ANN

models, for use in the field of slope stability assessment, in place of the traditional formula of the UB limit analysis method. Note that the GP formula was introduced as the more applicable formula due to its greater brevity and simplicity.

Compliance with Ethical Standards. Conflict of Interest: The authors declare that they have no conflict of interest.

References

1. Griffiths, D.V., Lane, P.A.: Slope stability analysis by finite elements. *Geotechnique* **49**, 387–403 (1999)
2. Taylor, D.W.: Stability of earth slopes. *J. Boston Soc. Civ. Eng.* **24**, 197–246 (1937)
3. Qian, Z.G., Li, A.J., Merifield, R.S., Lyamin, A.V.: Slope stability charts for two-layered purely cohesive soils based on finite-element limit analysis methods. *Int. J. Geomech.* **15**, 06014022 (2014)
4. Abuel-Naga, H.M., Bergado, D.T., Gniel, J.: Design chart for prefabricated vertical drains improved ground (reference no 2869). *Geotextiles Geomembranes* **43**, 537–546 (2015)
5. Aksoy, H.S., Gor, M., Inal, E.: A new design chart for estimating friction angle between soil and pile materials. *Geomech. Eng.* **10**, 315–324 (2016)
6. Moayed, H., Hayati, S.: Artificial intelligence design charts for predicting friction capacity of driven pile in clay. *Neural Comput. Appl.* **31** (2018, in press)
7. Samui, P., Kumar, B.: Artificial neural network prediction of stability numbers for two-layered slopes with associated flow rule. *Electron. J. Geotech. Eng.* **11**, 1–44 (2006)
8. Jellali, B., Frikha, W.: Constrained particle swarm optimization algorithm applied to slope stability. *Int. J. Geomech.* **17**, 06017022 (2017)
9. Jiang, X., Niu, J., Yang, H., Wang, F.: Upper Bound Limit Analysis for Seismic Stability of Rock Slope with Tunnel. *Advances in Civil Engineering* 2018 (2018)
10. Pan, Q., Dias, D.: Upper-bound analysis on the face stability of a non-circular tunnel. *Tunnelling Underground Space Technol.* **62**, 96–102 (2017)
11. Cramer, N.L.: A representation for the adaptive generation of simple sequential programs. In: *Proceedings of the First International Conference on Genetic Algorithms* (1985)
12. Koza, J.R.: Genetic programming as a means for programming computers by natural selection. *Stat. Comput.* **4**, 87–112 (1994)
13. Johari, A., Habibagahi, G., Ghahramani, A.: Prediction of soil–water characteristic curve using genetic programming. *J. Geotech. Geoenviron. Eng.* **132**, 661–665 (2006)
14. Makkeasorn, A., Chang, N.B., Beaman, M., Wyatt, C., Slater, C.: Soil moisture estimation in a semiarid watershed using RADARSAT-1 satellite imagery and genetic programming. *Water Resour. Res.* **42** (2006)
15. Garg, A., Garg, A., Tai, K., Sreedeeep, S.: An integrated SRM-multi-gene genetic programming approach for prediction of factor of safety of 3-D soil nailed slopes. *Eng. Appl. Artif. Intell.* **30**, 30–40 (2014)
16. Garg, A., Garg, A., Tai, K.: A multi-gene genetic programming model for estimating stress-dependent soil water retention curves. *Comput. Geosci.* **18**(1), 45–56 (2013). <https://doi.org/10.1007/s10596-013-9381-z>
17. Khandelwal, M., Marto, A., Fatemi, S.A., Ghoroghi, M., Armaghani, D.J., Singh, T.N., Tabrizi, O.: Implementing an ANN model optimized by genetic algorithm for estimating cohesion of limestone samples. *Eng. Comput.* **34**(2), 307–317 (2017). <https://doi.org/10.1007/s00366-017-0541-y>

18. McCulloch, W.S., Pitts, W.: A logical calculus of the ideas immanent in nervous activity. *Bull. Math. Biophys.* **5**, 115–133 (1943)
19. Jain, A.K., Mao, J., Mohiuddin, K.M.: Artificial neural networks: a tutorial. *Computer* **29**, 31–44 (1996)
20. Rao, S.G.: Artificial neural networks in hydrology. II: Hydrologic applications. *J. Hydrol. Eng.* **5**, 124–137 (2000)
21. El-Bakry, M.Y.: Feed forward neural networks modeling for K-P interactions. *Chaos, Solitons Fractals* **18**, 995–1000 (2003)
22. Moayed, H., Hayati, S.: Applicability of a CPT-based neural network solution in predicting load-settlement responses of bored pile. *Int. J. Geomech.* **18** (2018)
23. Florkiewicz, A.: Upper bound to bearing capacity of layered soils. *Can. Geotech. J.* **26**, 730–736 (1989)
24. Donald, I.B., Chen, Z.: Slope stability analysis by the upper bound approach: fundamentals and methods. *Can. Geotech. J.* **34**, 853–862 (1997)
25. Ranjbar Karkanaki, A., Ganjian, N., Askari, F.: Stability analysis and design of cantilever retaining walls with regard to possible failure mechanisms: an upper bound limit analysis approach. *Geotech. Geol. Eng.* **35**(3), 1079–1092 (2017). <https://doi.org/10.1007/s10706-017-0164-5>
26. Caër, T., Souloumiac, P., Maillot, B., Leturmy, P., Nussbaum, C.: Propagation of a fold-and-thrust belt over a basement graben. *J. Struct. Geol.* (2018)
27. Zhou, H., Liu, H., Yin, F., Chu, J.: Upper and lower bound solutions for pressure-controlled cylindrical and spherical cavity expansion in semi-infinite soil. *Comput. Geotech.* **103**, 93–102 (2018)
28. Moayed, H., Hayati, S.: Modelling and optimization of ultimate bearing capacity of strip footing near a slope by soft computing methods. *Appl. Soft Comput.* **66**, 208–219 (2018)
29. Koopialipoor, M., Jahed Armaghani, D., Hedayat, A., Marto, A., Gordan, B.: Applying various hybrid intelligent systems to evaluate and predict slope stability under static and dynamic conditions. *Soft. Comput.* **23**(14), 5913–5929 (2018). <https://doi.org/10.1007/s00500-018-3253-3>
30. Momeni, E., Armaghani, D.J., Hajihassani, M., Amin, M.F.M.: Prediction of uniaxial compressive strength of rock samples using hybrid particle swarm optimization-based artificial neural networks. *Measurement* **60**, 50–63 (2015)
31. Armaghani, D.J., Tonnizam Mohamad, E., Momeni, E., Monjezi, M., Sundaram Narayanasamy, M.: Prediction of the strength and elasticity modulus of granite through an expert artificial neural network. *Arabian J. Geosci.* **9**(1), 1–16 (2015). <https://doi.org/10.1007/s12517-015-2057-3>
32. Mohamad, E.T., Armaghani, D.J., Momeni, E., Yazdavar, A.H., Ebrahimi, M.: Rock strength estimation: a PSO-based BP approach. *Neural Comput. Appl.* **30**(5), 1635–1646 (2016). <https://doi.org/10.1007/s00521-016-2728-3>
33. Moayed, H., Jahed Armaghani, D.: Optimizing an ANN model with ICA for estimating bearing capacity of driven pile in cohesionless soil. *Eng. Comput.* **34**(2), 347–356 (2017). <https://doi.org/10.1007/s00366-017-0545-7>